Brodogradnja/Shipbilding/Open access Volume 73 Number 3, 2022

Xingkun Zhou
Jinghao Chen
Zhengguang Ge
Tong Zhao
Wenhua Li

http://dx.doi.org/10.21278/brod73301

ISSN 0007-215X
eISSN 1845-5859

NUMERICAL INVESTIGATIONS ON THE EFFECTS OF SEABED SHALLOW SOILS ON A TYPICAL DEEPWATER SUBSEA WELLHEAD SYSTEM

UDC 629.5.015.1:629.55:551.466.3
Original scientific paper

Summary

Deepwater subsea wellheads may be significantly threatened under extreme sea conditions and operations, especially when the seabed is composed of very soft clay properties. A numerical model of a deepwater wellhead system is established using the classic ocean pipe element and nonlinear spring element of ANSYS to examine the behaviors of subsea wellheads in diverse seabed soil. Nonlinear spring elements coded in the APDL language are used to model three types of seabed soils: very soft soil, soft soil, and firm soil. The dynamic and quasi-static behaviors of the wellhead system in the typical coupled and decoupled models of the drilling riser system are particularly investigated in depth. The effects of the nonlinear seabed soil properties on the detailed wellhead are realistically simulated using time domain and extremum analysis. The results show that the softer the seabed soil, the greater the displacement, rotation angle, curvature, and bending moment of deepwater subsea wellheads. When the seabed soil reaches a particular depth, the mechanical characteristics of the wellheads under the three types of seabed soil conditions are almost simultaneously close to zero. Overall, several conclusions reached in this study may provide some useful references for design and stability analysis.

Key words: Subsea wellhead; Seabed soil; Mechanical behaviour; Nonlinear spring

1. Introduction

Deepwater oil and gas drilling and production are important embodiments of marine resource development. The major key technical equipment for oil and gas exploration is the offshore drilling units, which include floating vessel, marine risers, and underwater wellhead. The stability of those key components is related to the safety and reliability of deepwater drilling operations. During drilling operations, the wellhead system and top casings are designed to support dynamic loads from the connected riser via the blowout preventer (BOP) and/or lower marine riser package (LMRP) [1, 2]. The wellhead is easily and inevitably

damaged due to a variety of factors, including the low-cycle and huge loads transmitted through the global riser system and the soil-casing weak interaction (especially in soft or very soft seabed soils) [4, 5, 6]. Currently, many studies are focusing on the hydrodynamic characteristics of floating units, as well as the static and dynamic behaviors, strength, and stability of riser joints [7, 8, 9, 10, 11]. However, those studies are focused on the global riser system rather than the detailed subsea wellhead.

Currently, conventional subsea wellhead system studies focus mainly on structural stability analysis and fatigue reliability evaluation. The time-domain and frequency-domain techniques were often used to investigate fatigue damage to critical components of top-hole casings and at the wellhead [2, 3]. Grytøyr et al [4] provided an indirect measurement-based technique for estimating bending moments at the wellhead. Li et al [6] studied the stability of a composite subsea wellhead, considering the effects of cement, waiting time, and riser joint end-resistance force. Kavanagh et al. [12] highlighted the analysis guidelines for modeling approaches of underwater wellhead systems and nonlinear subsea shallow soils. Reinås et al [13] used a fully developed fatigue fracture approach based on finite element method (FEM) analysis to calculate the residual ultimate load capacity of a typical North Sea subsea wellhead. Yan et al [14] investigated the underwater wellhead stability of a deepwater drilling riser using different top tension ratios under two drilling vessels' offsets. Deng et al [15] used numerical simulation and experimental methods to investigate the effects of mass force on the dynamics of a deepwater subsea wellhead system. Chang et al [16] used a proposed dynamic Bayesian networks methodology to evaluate the fatigue states and fatigue failure risk of a subsea wellhead system. Li et al [17] studied the fatigue damage of a subsea wellhead system using a novel semi-decoupled model developed using a local fine finite element approach. Wang et al [18, 19] used a dynamic failure analysis methodology based on finite element simulations to evaluate the reliability of subsea wellhead connectors and predict fatigue cracks. Jaculli et al [20] proposed a methodology for studying the problem of wellhead integrity and studied the effects of having a jetting base, setting a larger diameter conductor casing, and different well cementing designs on wellhead motions. Previous studies in the literature were more concerned with fatigue problems than the problem of excessive wellhead motions in different soft seabed soils. It should be noted that the problem of excessive wellhead motions can cause several well integrity problems, such as disruption of the cementing job (creation of channels during cement setting) and un-consolidation of the shallow formations (which could dislodge the conductor casing).

Deepwater seabed: shallow soil, as is often the case, has low strength and little resistance to lateral deflection [14]. Within 100 m of the deepwater seafloor, the shallow soil is usually clay [5]. A reliable structural model of a coupled soil-casing subsea wellhead system requires the lateral resistance of subsea soil at the mudline. However, the effects of deepwater seabed soft soils (especially shallow soil layers near the mudline) on the mechanical behaviors of underwater wellhead systems are rarely studied in the previous literature. As a result, the main objective of this study is to investigate the characteristics of a typical deepwater soil-casing coupled wellhead system by considering the three different types of deepwater seabed soils: very soft soil, soft soil, and firm soil, respectively, using recommendations and guidelines from the literature [21, 22, 23, 24, 25, 26]. The influence of subsea soils on the lateral displacement, rotational angle, curvature, bending moment, and shear of the deepwater subsea wellhead is investigated in detail. Overall, the investigations into the mechanical behaviors of laterally loaded conductor casing systems, as simulated by self-programming in ANSYS and Matlab, may improve the design of conductor casing systems and the prediction of lower flexible joint (LFJ) angles and wellhead bending moments [24].

2. Subsea wellhead and theoretical background

2.1 Wellhead modeling

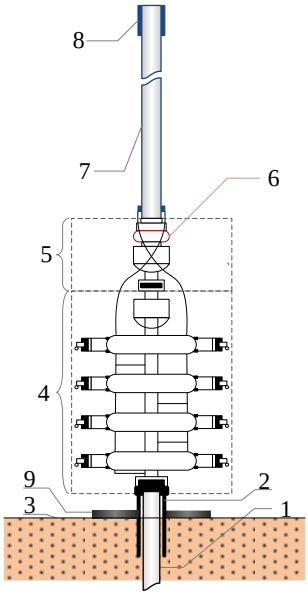

Fig. 1 Subsea wellhead system. (1) Casing, (2) conductor, (3) mudline, (4) blowout preventer, (5) lower marine riser package, (6) lower flex/ball joint, (7) marine riser, (8) buoyancy block, (9) mud mat.

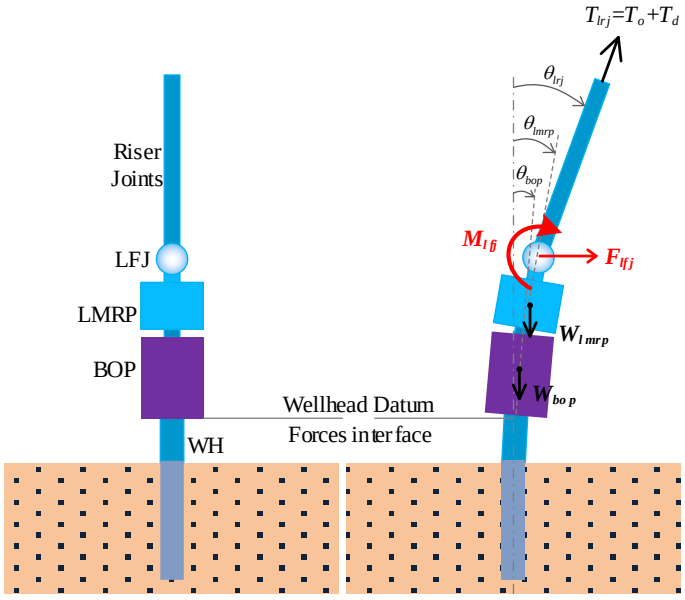

Fig. 2 Initial and deformed configurations of the subsea wellhead

As illustrated in Fig. 1, a marine wellhead system consists mainly of surface casings below the mudline, conductor casing, BOP, LMRP, LFJ, and a riser section above the mudline. The LMRP is typically comprised of a riser adapter, subsea control pods, and a hydraulic connector that links the riser system to the BOP. The BOP is normally located at the bottom of the LMRP and on the top of the conductor. The main function of the BOP is to shear the drill pipe and/or inner casing inside the riser main tube and close off the wall opening to prevent a blowout occurrence or to prepare for an emergency disconnect. The LFJ is capable of not only releasing bending moments caused by upper riser devices but also of

limiting a certain rotation angle (usually 2 to 4 degrees) [12, 14, 26] to prevent excessive string bending during normal drilling operations.

It is necessary to have information regarding the axial tension, bending moment, and shear force transmitted from the riser joints through the LFJ in the wellhead system. Fig. 2 illustrates the initial and deformed configurations of a wellhead system, where T_{lrj} is the tension of the lower riser joint (LRJ) directly above the LFJ, which consists of static T_o and dynamic T_d components, M_{lfj} and F_{lfj} are the bending moment and shear force, respectively, caused by the riser motion at the LFJ, W_{lmrp} and W_{bop} are the submerged weights of LMRP and BOP, and θ_{lrj}, θ_{lmrp} and θ_{bop} are the angles of LRJ, LMRP and BOP.

2.2 Wellhead and casing coupling

Because the LFJ bears certain loads from the above-mentioned decoupled riser system, its reaction can be seen as a loading point connected to the top end of the LMRP. According to the standard [26], the LMRP and BOP are two equivalent thick-walled pipe sections. The conductor and surface casings have the same external diameters but different wall thicknesses.

The wellhead and casing coupling system is modeled as a single rigid component with a regular geometric shape and homogeneous material properties [26]. Because, the conductor casing is jetted into the soil, it is directly subjected to soil lateral resistance. From the shoe to the wellhead, the surface casing is cemented and thus is bonded to the conductor casing. As shown in Fig. 3, the conductor casing is completely cemented onto the surface casing from the bottom of the BOP to 300 ft beneath the mudline.

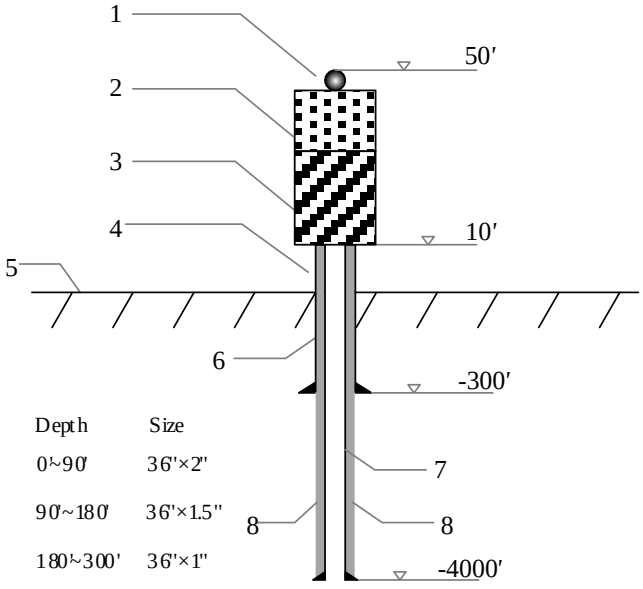

Fig. 3 The wellhead and casing system. (1) lower flex/ball joint, (2) lower marine riser package, (3) blowout preventer, (4) surface conductor, (5) mudline, (6) conductor casing, (7) surface casings, (8) cement.

The bending moment, shear force, and tension are usually extracted from the decoupled model of the structures between the LFJ and the upper flexible joint (UFJ) or a floating unit/vessel [6, 12, 13, 14, 26]. The wellhead constructors are modeled as linear elastic piles, and the interaction between the piles and the seabed soil is modeled as a pipe-soil coupled model. The soil is assumed to be elastoplastic, and a nonlinear spring model can be used to simulate the deformation feature of the seabed' shallow soil.

2.3 Soil-casing interaction modeling

The soil-casing interaction is modeled as a series of discrete, spaced, and nonlinear springs with a stiffness k_{soil} using the modified Winkler model theory and the theories in the literature [20, 26, 28, 29]. As illustrated in Fig. 4, each piece is modeled by a nonlinear spring. Constructing of lateral soil resistance-deflection (*p-y*) curves, with the ordinate of these curves being soil resistance per unit length *p* and the abscissa being lateral deflection *y*, can produce the typical soil behaviors. Using nonlinear spring models, the mechanical equilibrium equation of surface casing-soil coupled models can be derived. The structure's typical *p-y* behaviors can be expressed as [12],

$$EI\frac{d^4y}{dz^4} = p \tag{1}$$

where z is length along casing and *EI* is equivalent bending stiffness of casing system.

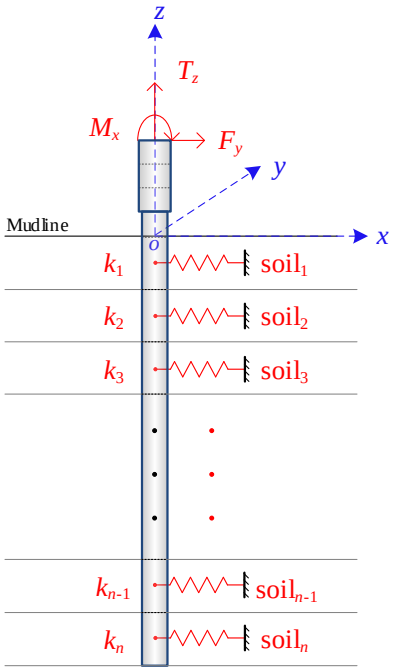

Fig. 4 Mechanical model of the wellhead system
where T_z, M_x, and F_y are the tension, bending moment, and shear, respectively.

Eq. (1) is obviously solvable if the only unknown physical quantity, soil resistance *p*, is obtained. However, the soil resistance, *p* is a nonlinear, complex function of soil depth and soil properties. Therefore, the primary task of the following study is to determine the soil resistance *p* of the surface casings in different shallow seabed soils.

The accurate prediction of the lateral deformation of loaded conductor casings embedded in soil is a critical factor in predicting the LFJ rotation angle and wellhead bending moment, which are important in wellhead system design. The soil strength below the mudline is generally low, resulting in little resistance to lateral deflections, and the area of greatest bending of the structural casing can thus occur some distance below the mudline. Therefore, determining the lateral resistance of the soil is an important input into developing a reliable structural model of a casing-soil coupled wellhead system.

Under lateral loading, clay soils generally behave as plastic materials, necessitating the correlation of pile-soil deformation to soil resistance. To make this procedure easier, lateral soil *p-y* curves should be examined first for construction using stress-strain data from

laboratory soil samples. In the absence of more definitive criteria, typical *p-y* curves procedures are recommended for calculating the ultimate lateral bearing capacity of subsea shallow soils. The ultimate unit lateral bearing capacity of soft clay p_u varies between 8*c* and 12*c* for static lateral loads, especially at shallow depths when failure occurs in a different mode due to minimum overburden pressure.

According to this, in the absence of more definitive criteria, p_u in the seabed shallow soft soils increases from 3*c* to 9c as *X* increases from 0 to X_R,

$$\begin{cases} p_u = 3c + \gamma X + J\dfrac{cX}{D} & \text{for} \quad (X < X_R) \\ p_u = 9c & \text{for} \quad (X \geq X_R) \end{cases} \tag{2}$$

and p_u in the subsea shallow hard soils increases from 2*c* to 9c,

$$\begin{cases} p_u = 2c + \gamma X + 2.83\dfrac{cX}{D} & \text{for} \quad (X < X_R) \\ p_u = 9c & \text{for} \quad (X \geq X_R) \end{cases} \tag{3}$$

where p_u is ultimate resistance, kPa; *c* is undrained shear strength for undisturbed clay soil samples, kPa; *D* is pipe outer diameter, mm; γ is effective unit weight of soil, MN/m^3; *J* is dimensionless empirical constant with values ranging from 0.25 to 0.5 that depends on soil stiffness, and a value of 0.5 is given in this study; *X* is depth below soil surface, mm; X_R is depth below soil surface to bottom of reduced resistance zone, mm, which is expressed as,

$$X_R = \frac{6D}{\dfrac{\gamma D}{c} + J} \tag{4}$$

Because drilling in sandy soil is rarely encountered in deepwater shallow formation (within100 m), the ultimate resistance strength p_u of sandy soil is omitted in this paper.

The undrained shear strength *c* and effective unit weight γ of the subsea shallow soils along depth referring to the literature [14, 20, 23, 26, 29] are listed in Table 1.

The *p-y* curves in soft clay are generally nonlinear for the short-term static load situation and may be generated by the following:

p/p_u	y/y_c
0.00	0.0
0.50	1.0
0.72	3.0
1.00	8.0
1.00	∞

where y_c is the displacement value when loading reaches half of the ultimate soil resistance.

$$y_c = 2.5\varepsilon_c D \tag{5}$$

where ε_c is the strain value that occurs at one-half the maximum stress in a laboratory undrained undisturbed soil test. The values of ε_c according to the different soils are given in the literature [20, 21, 26, 30], as shown in Table 2.

Table 1 Properties of the seabed shallow soils

Conditions	Measuring point (m)	c (kPa)	γ (kN/m^3)
Case I:	0	2.390	3.120
Very soft soil	-9.14	4.575	3.342
	-91.44	38.070	5.340
Case II:	0	13.533	3.120
Soft soil	-9.14	16.676	3.435
	-91.44	64.847	6.274
Case III:	0	27.857	3.120
Firm soil	-9.14	31.934	3.529
	-91.44	94.420	7.208

Table 2 Values of ε_c for different types of seabed soils

Soil	ε_c
Very soft	0.020
Soft	0.010
Firm	0.005

As illustrated in Fig. 5, data from the *p-y* curve referring to the standard ISO/TR-2009 [26] are plotted and fitted using regression techniques.

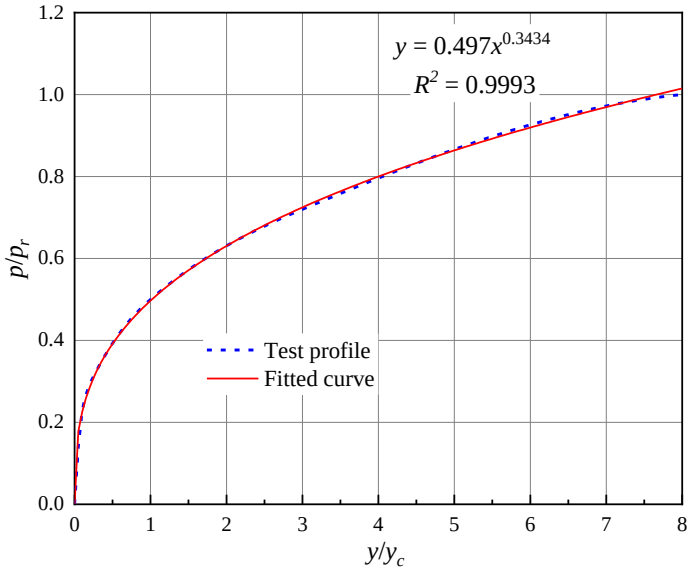

Fig. 5 Typical *p-y* curve for seabed soils. The solid line is plotted data (test profile) referring to ISO/TR-2009, while the dotted line is fitted data. R^2 is very close to 1 and confirms a good fit.

Eq. 6 expresses the *p-y* relationship, and Eq. 7 expresses the soil stiffness k_{soil}, with a comparison of k_{soil} between Jaculli et al [20] and this study.

$$\frac{p}{p_u} = 0.497\left(\frac{y}{y_c}\right)^{0.3434} \tag{6}$$

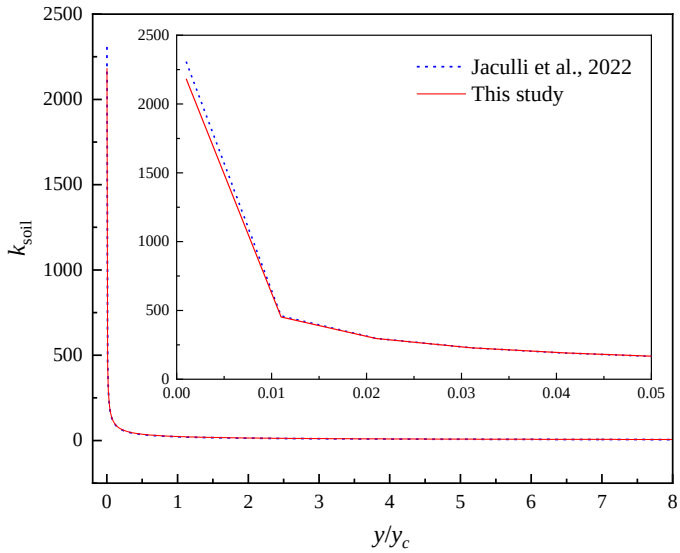

Fig. 6 Comparison of the soil stiffness k_{soil} between the literature and this study.

$$k_{soil}(y)=\frac{dp}{dy}=\frac{0.1706698p_u\Delta x}{(y/y_c)^{0.6566}}0.497^{0.3434} \tag{7}$$

where Δx is the length of the soil segment since the representative lateral soil capacity p has units of force per length.

The subsea shallow soil will be subjected to periodic loading after the balance of short-term static loading. The lateral resistance strength usually decreases and is less than the static resistance strength. According to the literature [20-22, 26], periodic loading can lower soil lateral ultimate resistance strength to 0.72 P_u.

3. Methodology

3.1 Coupled model versus decoupled model

Fig. 7 illustrates the overall system under consideration in this study. The global model comprises all the structural components of the drilling system, including the soil and the wellhead itself. Because of the irregular waves, the drill deck floats on the surface and experiences heave, surge, sway, pitch, and roll motions [27]. To simulate the riser system's heave motion, an equivalent spring with stiffness k_c is used herein, and the time-varying top tension $T_t(t)$ can be expressed as,

$$T_t(t)=T_o+T_d=fw_eL+k_ca\cos(\omega_d t) \tag{8}$$

where T_o is the static pretension; T_d is the dynamic component; T_o can be determined by the pretension factor f, the submerged weight of riser per unit length w_e, and the riser total length L; a and ω_d are the amplitude and frequency of platform heave motion; k_c is defined by [7],

$$k_c=w_eL/a_c \tag{9}$$

where a_c is the critical amplitude, usually set at 10 m.

The coupled model contains the vessel (modeled implicitly), the flex joints, the riser joints, the LMRP/BOP, the casings, and the soil. The wellhead system can also be seen as the coupled model's lower end boundary condition [20].

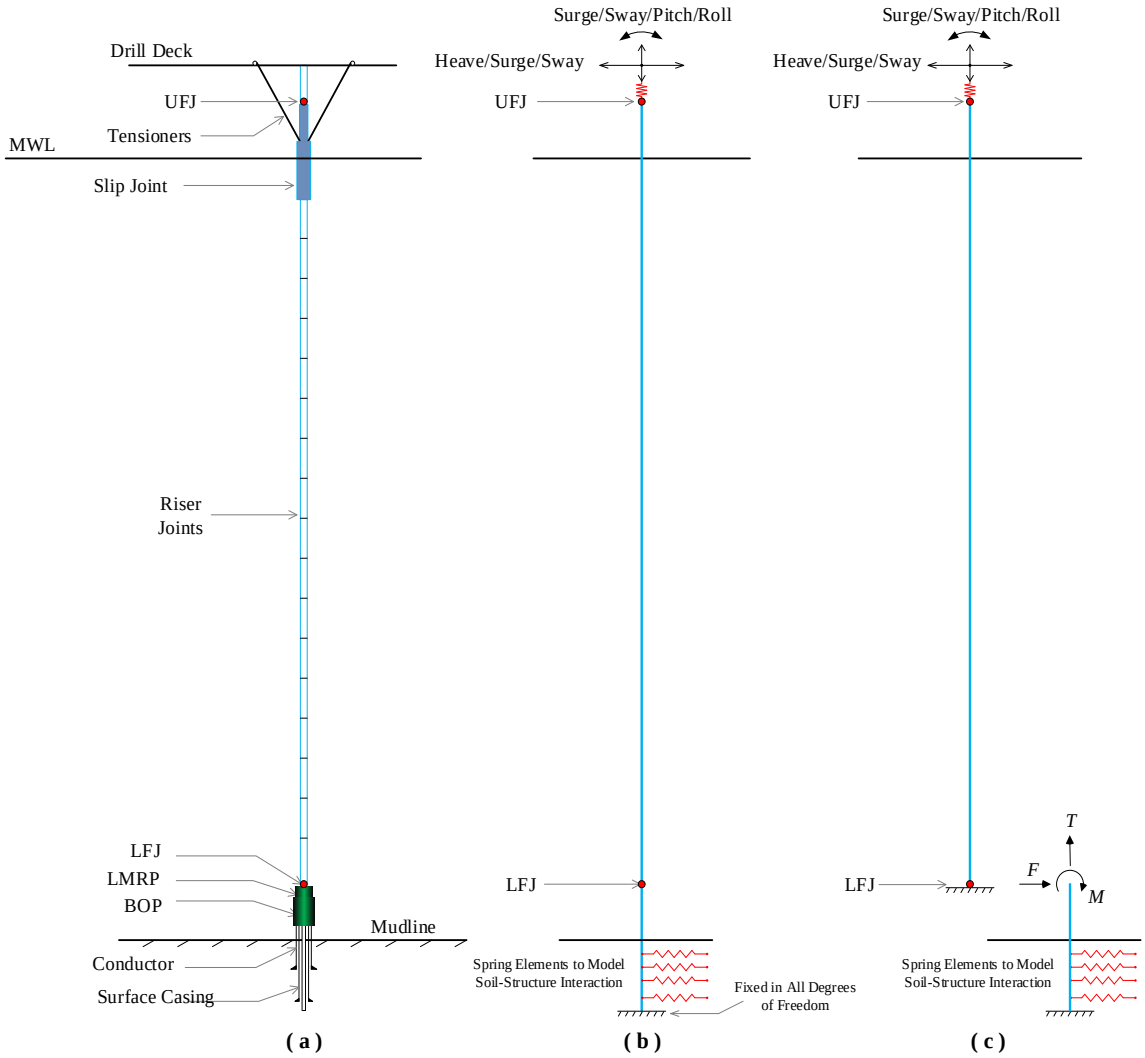

Fig. 7 Global analysis for the coupled and decoupled models of a deepwater drilling riser. (a) the entire system model, (b) the typical coupled model, (c) the typical decoupled model.

The wellhead casing, and soil are modeled separately as an equivalent system in the decoupled model. Axial tension *T*, bending moment *M*, and shear force *F* are the primary loads transmitted from the riser joints to the wellhead via the LFJ [14, 20].

In comparison, coupled analysis is a better method to use when the conductor/casing response is a key output, such as in the design of the wellhead system [12]. While the decoupled analysis is simpler to model and solve, it takes less time [20]. The modeling and results of the two methodologies are studied in detail in the following section, and the benefits are again re-checked in Section 4.

3.2 FEM coded in APDL

In ANSYS, PIPE288 is a typical ocean-loading element that can account for the effects of waves, current, drag, and buoyancy. The loading is input globally using the ocean family of commands, such as OCTYPE, OCDATA, and OCTABLE, coded in ANSYS Parametric Design Language (APDL). The PIPE288 element can be used to identify wellhead system structures including LMRP/BOP, conductor casing, and surface casing. It is based on Timoshenko beam theory and is widely used in marine risers and pipelines because of its good ocean function module support. Many studies have employed this element to solve various problems. There is no need to repeat this.

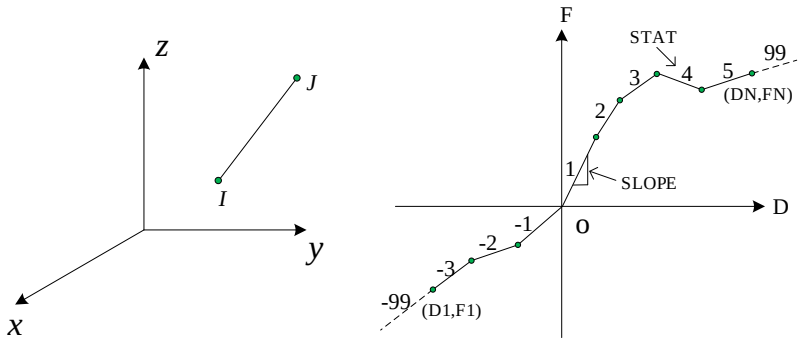

Fig. 8 D–F curve of the typical COMBIN39 spring element.

Nonlinear COMBIN39 elements can be used to model subsea shallow soils. A nonlinear spring element with variable stiffness k_{soil} can be used to simulate each layer of the soil body. Every element has a longitudinal function that represents axial tension or compression. As illustrated in Fig. 8, the element is defined by two node points and a generalized force-deflection curve. When there is only one soil undrained shear strength parameter, the soil can be seen as an elastic-perfectly plastic material. The element force-deformation curve can be derived using the points (D, F) and the origin (0,0) and then modeled and solved. The slope of the curve in the elastic stage is the nonlinear spring stiffness k_{soil} of different soil layers. As a result, calculating the soil stiffness k_{soil} versus lateral loading-deflection and soil depth is crucial.

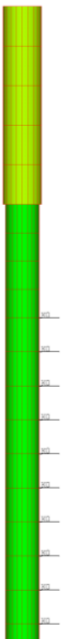

Fig. 9 Finite element model of the wellhead system in ANSYS software.

The direct node-element modeling method can be used to model the wellhead structures. As illustrated in Fig. 4, the origin in the Cartesian coordinate system is set at the junction of the conductor and surface casing, the *xoy* plane is the seabed, and the *z* axial positive direction is seabed up. Using the PIPE288 element, each component of the wellhead system is uniformly discretized into several units. The two nonlinear spring element nodes are located along the *x* axis and perpendicular to the axial direction of the surface casings, with one node is shared with the casing element and the other as a fixed end (with non-freedom degree). Finally, the numerical model of the wellhead system is constructed using APDL. The continuous strength profile of the subsea shallow soil is efficiently valuated using the loop

statement language, and the finite element simulation model of the wellhead system is developed, as shown in Fig. 9.

3.3 Case studies

A typical deepwater drilling riser system in the South China Sea is taken as an example to investigate the stability of the wellhead under different soil conditions. Table 3 lists the main properties of the entire riser system.

Table 3 The main properties of the entire drilling riser system

Component	Variable		Value	Unit
Environment	ρ_w	Seawater density	1025.5	kg/m^3
	H_s	Significant wave height	4	m
	T_p	Peak period	8	s
	U_0	Current speed at the surface	0.5	m/s
	g	Gravitational acceleration	9.81	m/s2
Platform	a	Amplitude of platform heave motion	2	m
	ω_d	Frequency of platform heave motion	0.9604	rad/s
Riser	L_r	Riser length	3048	m
	D_{or}	Riser outer diameter	0.5334	m
	D_{ir}	Riser inner diameter	0.489	m
	E_r	Riser Young's modulus (steel)	210	GPa
	ρ_r	Riser density (steel)	7850	kg/m^3
	ρ_f	Inner fluid density	1200	kg/m^3
	f	Riser top tension (as a factor of weight)	1.3	-
	C_a	Riser added mass coefficient	1.0	-
	C_d	Riser drag coefficient	1.2	-
	G_{ufj}	Upper flex joint rotational stiffness	338	kN.m/◦
	G_{lfj}	Lower flex joint rotational stiffness	127.4	kN.m/◦
LMRP	L_{lmrp}	Stack height	3.66	m
	W_{lmrp}	Wet weight	1094	kN
	D_{olmrp}	Outer diameter	1.035	m
	D_{ilmrp}	Inner diameter	.476	m
BOP	L_{bop}	Stack height	8.53	m
	W_{bop}	Wet weight	1642	kN
	D_{obop}	Outer diameter	1.035	m
	D_{ibop}	Inner diameter	0.476	m
Surface casing	L_{sc}	Surface casing length	1219.2	m
	D_{os}	Surface casing outer diameter	0.762	m
	D_{is}	Surface casing inner diameter	0.6858	m
Cement	E_c	Cement Young's modulus	30	GPa
Soil	γ	Soil submerged unit weight	7	kN/m^3
	c_u	Soil undrained shear strength	60	kPa
	J	Soil empirical constant	0.5	-
Simulation	N_r	Number of riser elements	500	-
	t_t	Total simulation time	600	s
	Δt	Time step	0.1	s
	N_{cc}	Number of conductor casing elements	110	-

Note: the diameter and stiffness of LMRP/BOP are the equivalent properties referring to ISO/TR 13624-2 [26].

Table 4 shows three types of conductor casing according to the designed wall thickness.

Table 4 The main properties of the conductor casings

Item	Depth m (ft)	Outer diameter, cm (in)	Wall thickness, cm (in)
Conductor casing I	3.0 ~ -27.4 (0 ~ -90)	91.44 (36)	5.08 (2.0)
Conductor casing II	-27.4 ~ -54.9 (-90 ~ -180)	91.44 (36)	3.81 (1.5)
Conductor casing III	-54.9 ~ -91.4 (-180 ~ -300)	91.44 (36)	2.54 (1.0)

4. Results and discussions

The results obtained by self-coding in this study are similar to those found in the literature [13, 14, 20], demonstrating the computation's validity. The complicated ocean environment is defined by the irregular JONSWAP waves and constant current. The overall computation time is 600 s, with each time iteration step lasting 0.1 s.

Because deformations such as lateral displacement and cross-section angle at the top end of the conductor casing (beneath the BOP) are key outputs in wellhead design, the lateral displacement and rotation angle at the particular point vary with time and need to be monitored more closely. Figs. 10 and 11 illustrate the time-domain displacements and angles of the conductor casing in the coupled and decoupled models under three different kinds of typical seabed soils.

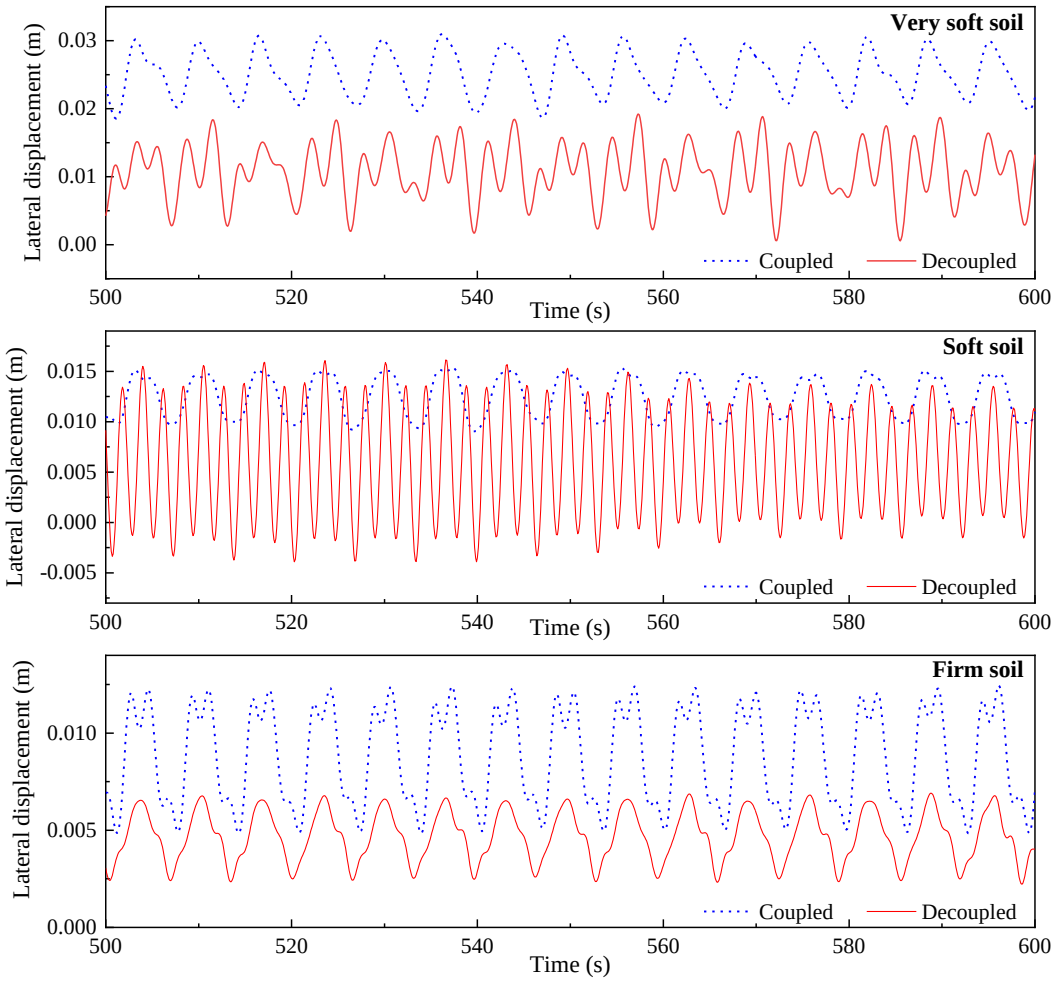

Fig. 10 The time domain lateral displacement at the wellhead top end under different subsea shallow soils.

Figs. 10 and 11 show that the amplitudes of the time-domain lateral displacement and angle of the decoupled model are larger than those of the global coupled model under the very soft soil and soft soil conditions. However, when the subsea shallow soil is firm, the same behavior occurs in the other direction. Furthermore, the time-domain deformations of the coupled and decoupled models show resonance periodicity.

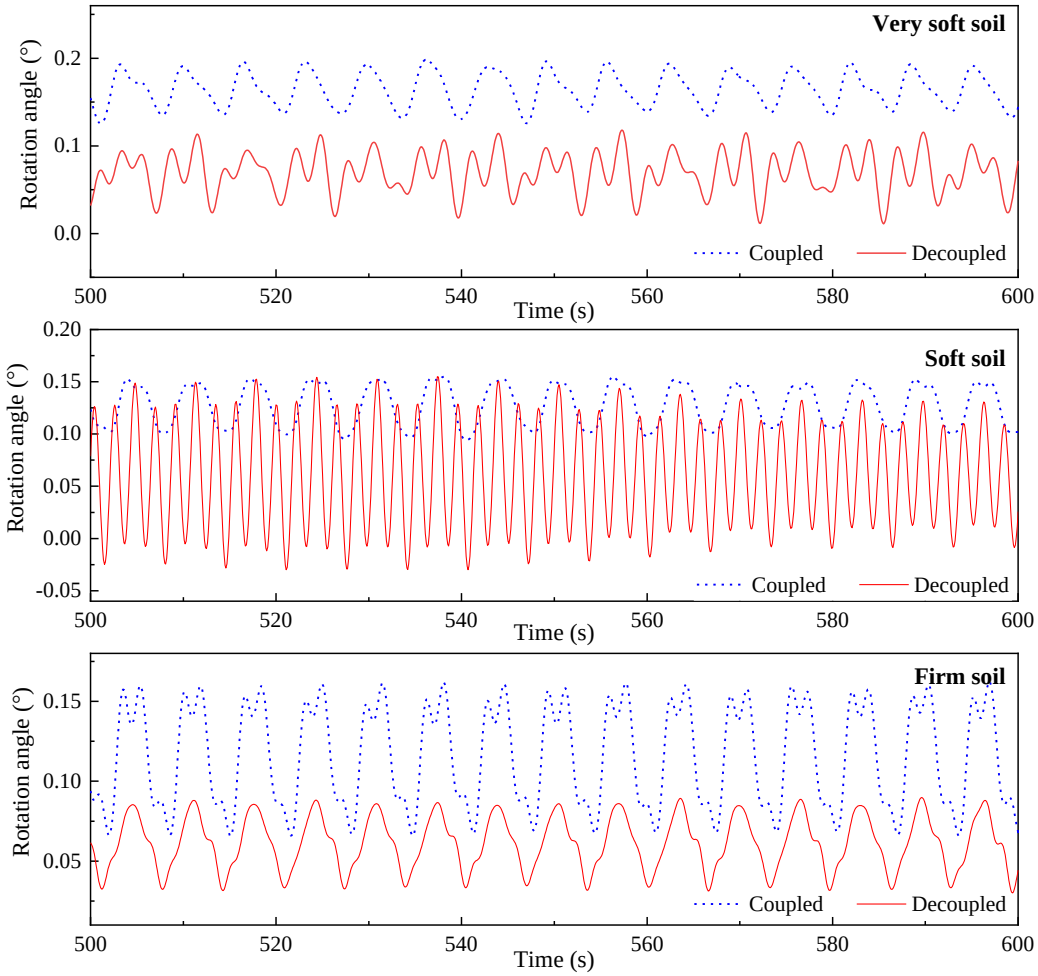

Fig. 11 The time domain cross-section angle at the wellhead top end under different subsea shallow soils.

According to the results in Figs. 10 and 11, the coupled model may provide better results, but it is more complex to model and takes longer to solve, as studied by Jaculli et al [20]. Therefore, the decoupled model is discussed in detail below.

Table 5 Maximum loads of the wellhead system

Soil	Parameter	Value	Unit
Very soft	M_{max} Maximum bending moment	118.1	kN.m
	F_c Corresponding shear	15.5	kN
	T_c Corresponding tension	15056.9	kN
Soft	M_{max} Maximum bending moment	169.6	kN.m
	F_c Corresponding shear	21.8	kN
	T_c Corresponding tension	15357.2	kN
Firm	M_{max} Maximum bending moment	258.9	kN.m
	F_c Corresponding shear	25.0	kN
	T_c Corresponding tension	17146.3	kN

The time domain axial tension *T*, bending moment *M*, and shear force *F* are extracted (as shown in Fig. 12) as the key inputs for the wellhead system design. According to the literature [14, 20], the maximum moment at the LFJ, as well as the accompanying tension and shear, are critical and are presented in Table 5.

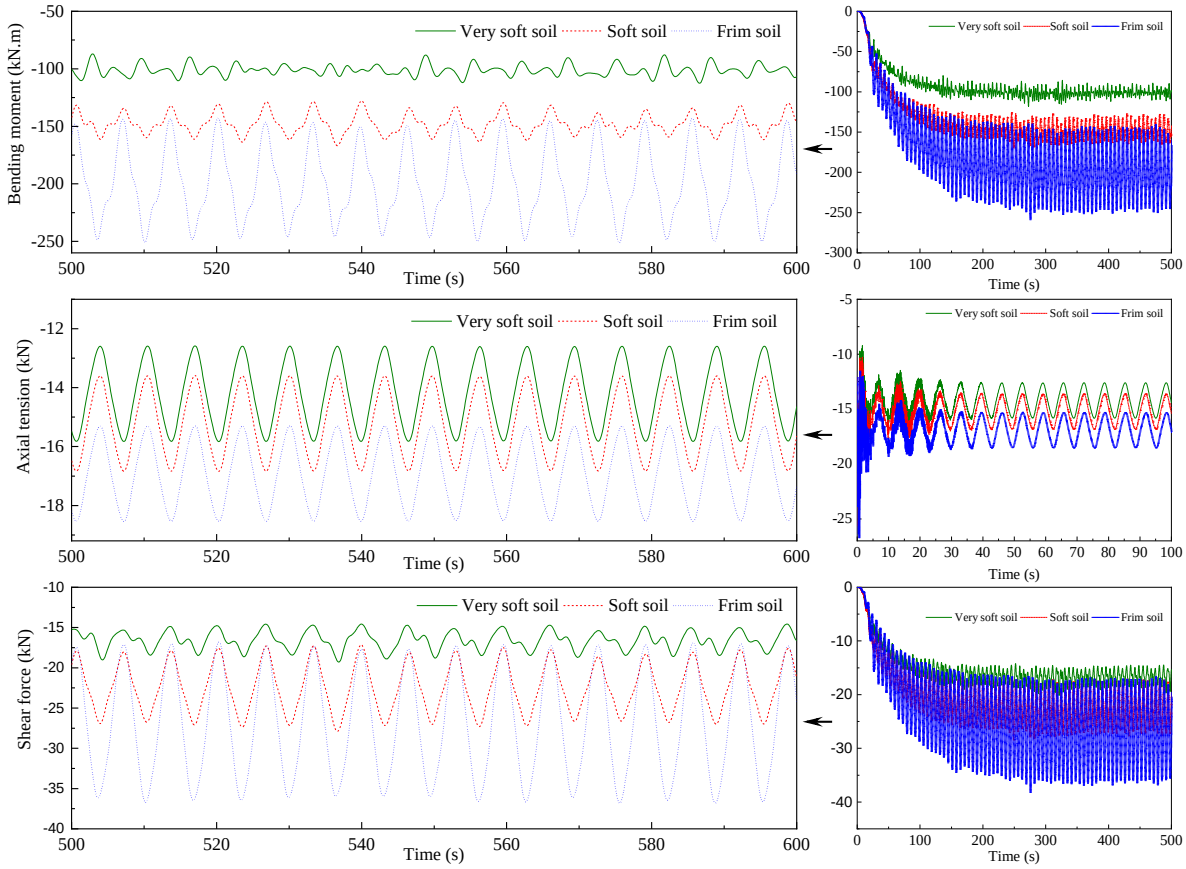

Fig. 12 The time domain force states at the LFJ under different subsea shallow soils.

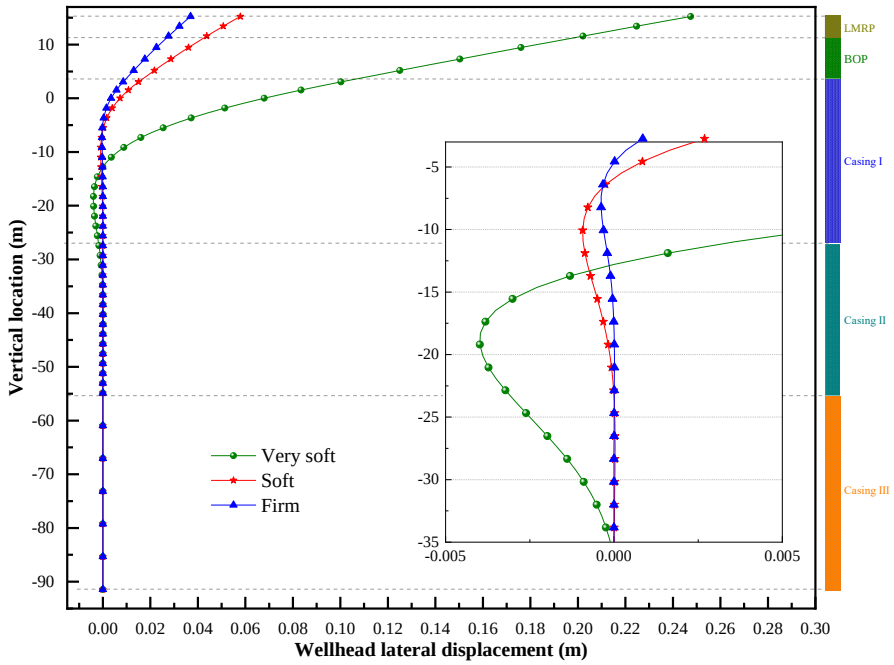

Fig. 13 The wellhead horizontal displacements under different subsea shallow soils.

The maximum deformation and mechanical states should be rechecked in the wellhead system design with the transmitted loads from the decoupled riser system loading. The quasistatic studies are conducted utilizing the maximum loads from Table 4. Figs. 12–16 illustrate the lateral displacements, angles, curvatures, bending moments, and shears versus soil depth.

Fig. 13 illustrates that the maximum lateral displacement of the wellhead is respectively about 0.25, 0.06, and 0.04 m under the very soft soil (Case I), the soft soil (Case II), and the firm soil (Case III) conditions. The minimum displacement of the wellhead occurs under the mudline. The softer the subsea soil, the smaller the negative displacement, and the deeper the position of the minimum displacement. When the soil reaches a certain depth (in this case the computation depth is about 35 m below the mudline), the displacement of the wellhead is close to zero.

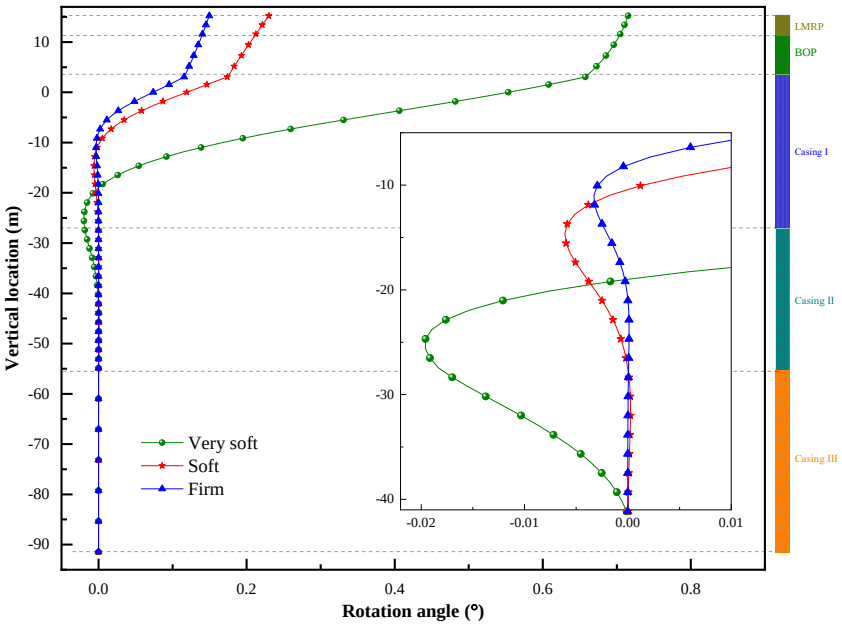

Fig. 14 The wellhead cross-section angles under the different subsea soils.

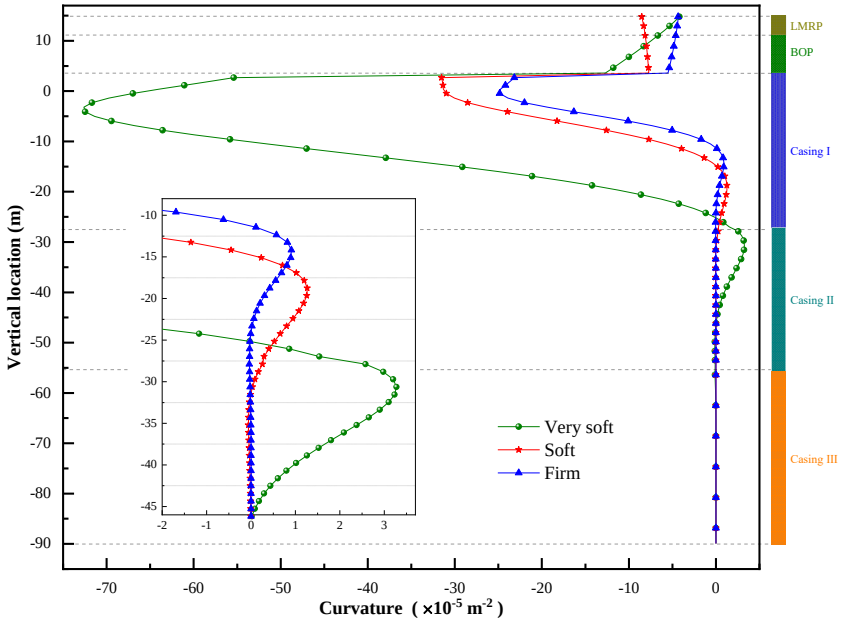

Fig. 15 The wellhead curvature under different subsea shallow soils.

Fig. 14 illustrates that the softer the seabed shallow soil, the lower the position of the minimum angle of the wellhead. When the soil depth is about 40 m below the mudline, the rotation angle of the wellhead is close to zero.

Fig. 15 illustrates the curvatures under the different subsea shallow soils. The maximum curvature occurs beneath the mudline. The curvature is close to zero when the soil depth is about 45 m.

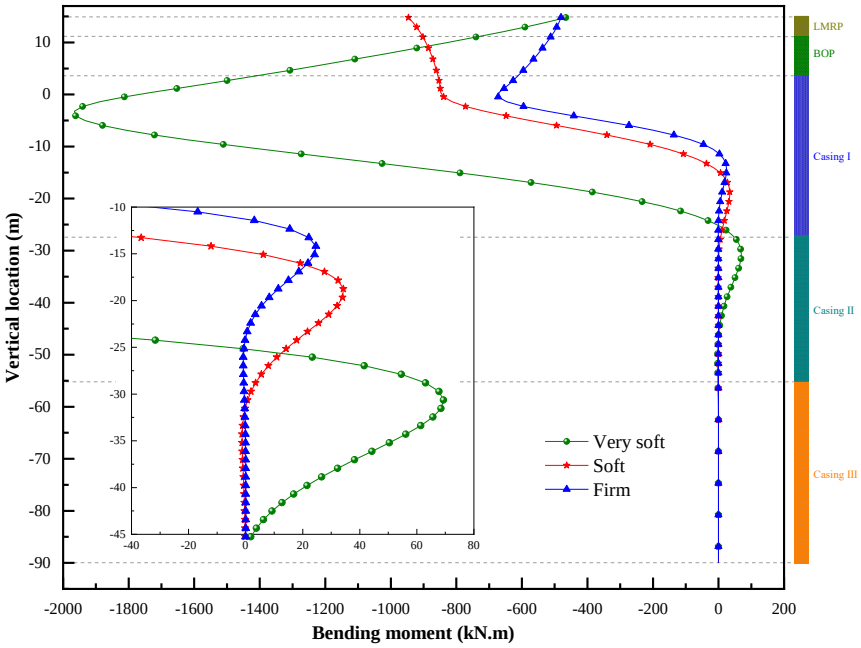

Fig. 16 Bending moments of the wellhead system under the different subsea shallow soils

Fig. 16 illustrates that the softer the soil, the greater the bending moment, and the deeper the position of the maximum bending moment. The bending moment tends to zero when the soil depth is about 45 m under the mudline.

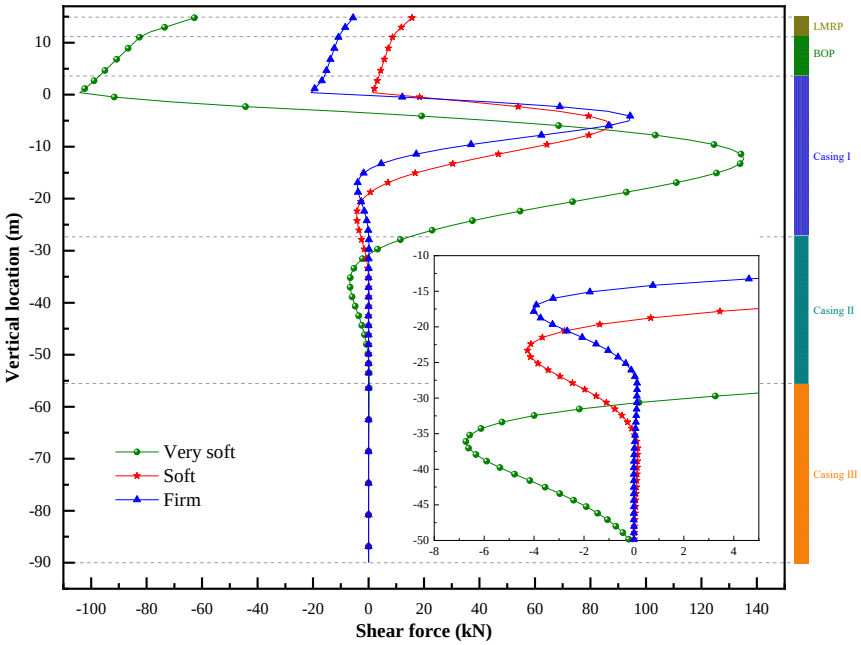

Fig. 17 Shears of the wellhead system under the different subsea shallow soils

Fig. 17 illustrates that the extreme shears of the wellhead occur at the top end of the conductor and at a certain depth below the mudline. The softer the soil, the larger the amplitude of the shear, and the deeper the position of the amplitude of the shear. When the soil depth is about 50 m under the mudline, the shear tends to zero.

5. Conclusions

The analysis of the coupled entire model and the decoupled local model, which are built in ANSYS using the unique ocean-loading supporting element PIPE288, is used to study a deepwater subsea wellhead system. The nonlinear spring element COMBIN 39 is used to mimic the complex mechanical properties of subsea shallow soils. The time-domain response, as well as the extreme deformation and force states of the wellhead system are studied in different typical subsea soils.

The shallow seabed soils have a significant impact on the lateral displacement and cross-section angle of the subsea wellhead system. Under very soft and soft soil, the time-domain deformation of the global coupled model is smaller than that of the decoupled model, but under firm soil, the opposite phenomenon occurs. As a result, the decoupled model is (is not) more conservative for soft (hard) soil as compared to the standard [20, 26].

The greater the value of wellhead deformation, the softer the seafloor shallow soil. When the soil reaches a certain depth, deformations, such as lateral displacement and rotation angle, as well as force states such as bending moment and shear, are close to zero when the soil reaches a certain depth. However, the critical depth of the soil will not exceed 50 m in any event, indicating that the fixed end assumption of the wellhead-casing-soil model under the mudline of 91.44 m is entirely reasonable and is consistent with the literature [14, 20].

In a future study, a compromise between the coupled and the decoupled models could be considered to provide an equivalent linear or nonlinear spring to simulate the effect of different subsea soil resistances on the decoupled wellhead system.

ACKNOWLEDGEMENT

This work is supported by the National Natural Science Foundation of China (Grant No. 52001044), the Open Project Program of Beijing Key Laboratory of Pipeline Critical Technology and Equipment for Deepwater Oil & Gas Development (Grant No. BIPT2021001), the Fundamental Research Funds for Central Universities (Grant No. 3132022348), the subproject of MIIT's high-tech Ship Scientific Research Plan (Grant No. [2018]473), the Liaoning Provincial Natural Science Foundation of China (Grant No. 2020-HYLH-35), and the 111 Project (Grant No. B18009).

REFERENCES

[1] Du, J., Li, X., Bao, H., Xu, W., Wang, Y., Huang, J., Wang, H., Wanyan, R., Wang, J., 2019. Geological conditions of natural gas accumulation and new exploration areas in the Mesoproterozoic to Lower Paleozoic of Ordos Basin, *Petroleum Exploration and Development*. 46(5), 866-882. https://doi.org/10.1016/S1876-3804(19)60246-6

[2] Rezende, F. A., Lopes, G. K., Sousa, F. J. M., Sousa, J. R. M., Fonseca, C. E., Percy, J. G., 2020. Wellhead Fatigue Analysis Considering Global and Local Effects. *Proc. ASME. OMAE2020, Volume 4: Pipelines, Risers, and Subsea Systems*, OMAE2015-41379. https://doi.org/10.1115/OMAE2020-18854

[3] Kim, S. W., Liu, S., Lee, S. J., 2020. Development of a new fatigue damage model for quarter-modal spectra in frequency domain. *Brodogradnja*. 71, 39-57. https://doi.org/10.21278/brod71103

[4] Grytøyr, G., Coral, F., Lindstad, H. B., Russo, M., 2015. Wellhead Fatigue Damage Based on Indirect Measurements. *Proc. ASME. OMAE2015, Volume 5B: Pipeline and Riser Technology*, Volume 5B: OMAE2015-41379. https://doi.org/10.1115/OMAE2015-41379

[5] Chang, Y., Jiang, Y., Zhang, C., Xue, A., Chen, B., Zhang, W., Xu, L., Liu, X., Dai, Y., 2021. PERT based emergency disposal technique for fracture failure of deepwater drilling riser. *Journal of Petroleum Science and Engineering*. 201, 108407. https://doi.org/10.1016/j.petrol.2021.108407

[6] Li, W., Gao, D., Yang, J., Hu, Z., Abimbola, F., 2020. Subsea wellhead stability study of composite casing for deepwater drilling. *Ocean Engineering*. 214, 107780. https://doi.org/10.1016/j.oceaneng.2020.107780

[7] Lei, S., Zheng, X. Y., Kennedy, D., 2017. Dynamic response of a deepwater riser subjected to combined axial and transverse excitation by the nonlinear coupled model. *International Journal of Non-Linear Mechanics*. 97, 68-77. https://doi.org/10.1016/j.ijnonlinmec.2017.09.001

[8] Zhou, X., Sun, Y., Duan, M., Li, W., 2020. Numerical investigation on crack identification using natural frequencies and mode shapes of a drilling riser during deployment and retrieval. *Journal of Petroleum Science and Engineering*. 195, 107721. https://doi.org/10.1016/j.petrol.2020.107721

[9] Chang, Y., Zhang, C., Xu, X., Shi, J., Chen, G., Ye, J., Xu, L., Xue, A., 2019. A Bayesian Network model for risk analysis of deepwater drilling riser fracture failure. *Ocean Engineering*. 181, 1-12. https://doi.org/10.1016/j.oceaneng.2019.04.023

[10] Zhang, N., Chang, Y., Shi, J., Chen, G., Zhang, S., Cai, B., 2021. Fragility assessment approach of deepwater drilling risers subject to harsh environments using Bayesian regularization artificial neural network. *Ocean Engineering*. 225, 108793. https://doi.org/10.1016/j.oceaneng.2021.108793

[11] Liu, X., Liu, Z., Wang, X., Zhang, N., Qiu, N., Chang, Y., Chen, G., 2021. Recoil control of deepwater drilling riser system based on optimal control theory. *Ocean Engineering*. 225, 108793. https://doi.org/10.1016/j.oceaneng.2020.108473

[12] Kavanagh, K., Dib, M., Balch, E., Stanton, P., 2002. New Revision of Drilling Riser Recommended Practice (API RP 16Q). In: presented at the *Offshore Technology Conference*, Houston, Texas, May 2002. OTC-14263-MS. https://doi.org/10.4043/14263-MS

[13] Reinås, L., Sæther, M., Aadnøy, B. S., 2012. The Effect of a Fatigue Failure on the Wellhead Ultimate Load Capacity. *Proc. ASME. OMAE2012, Volume 1: Offshore Technology*, Rio de Janeiro, Brazil. July 1–6, 2012. OMAE2012-83325. https://doi.org/10.1115/OMAE2012-83325

[14] Yan, W., Chen, Z., Deng, J., Zhu, H., Deng, F., Liu, Z., 2015. Numerical method for subsea wellhead stability analysis in deepwater drilling. *Ocean Engineering*. 98, 50-56. https://doi.org/10.1016/j.oceaneng.2015.02.007

[15] Deng, S., Liu, Y., Jiang, P., Zhu, S., Tao, L., He, Y., 2019. Simulation and experimental study of deepwater subsea wellhead-shallow casing deflection considering system mass force. *Ocean Engineering*. 187, 106222. https://doi.org/10.1016/j.oceaneng.2019.106222

[16] Chang, Y., Wu, X., Zhang, C., Chen, G., Liu, X., Li, J., Cai, B., Xu, L., 2019. Dynamic Bayesian networks based approach for risk analysis of subsea wellhead fatigue failure during service life. *Reliability Engineering & System Safety*. 188, 454-462. https://doi.org/10.1016/j.ress.2019.03.040

[17] Li, J., Chang, Y., Xiu, Z., Liu, H., Xue, A., Chen, G., Xu, L., Sheng, L., 2020. A local stress-strain approach for fatigue damage prediction of subsea wellhead system based on semi-decoupled model. *Applied Ocean Research*. 102, 102306. https://doi.org/10.1016/j.apor.2020.102306

[18] Wang, Y., Liu, S., Chen, Z., Wang, M., Yang, J., Chen, X., 2021. Dynamic Bayesian networks for reliability evaluation of subsea wellhead connector during service life based on Monte Carlo method. *Journal of Loss Prevention in the Process Industries*. 71, 104487. https://doi.org/10.1016/j.jlp.2021.104487

[19] Wang, Y., Chen, Z., Yan, Q., Hu, Y., Wang, C., Luo, W., Cai, B., 2022. A dynamic failure analysis methodology for fault diagnosis of fatigue cracks of subsea wellhead connectors with material aging. *Process Safety and Environmental Protection*. 159, 36-52. https://doi.org/10.1016/j.psep.2021.12.044

[20] Jaculli, M. A., Mendes, J. R. P., Colombo, D., 2022. Evaluation of excessive wellhead motions: Framework of analysis and case studies (Part I). *Journal of Petroleum Science and Engineering*. 208, C, 109571. https://doi.org/10.1016/j.petrol.2021.109571

[21] Liu, W., Guan, H., Zhou, Q., Lou, J., 2021. Study on structural-acoustic characteristics of cylindrical shell based on wavenumber spectrum analysis method. *Brodogradnja*. 72(2), 57-71. http://dx.doi.org/10.21278/brod72204

[22] API RP 2A-WSD, 2014. Planning, Designing, and Constructing Fixed Offshore Platforms—Working Stress Design, Twenty-second Edition.

[23] DNV-RP-F105, 2017. Recommended Practice: Free Spanning Pipelines.

[24] Dominguez, F., Carral, L., 2020. A review of formulations to design an adhesive single-lap joint for use in marine applications. *Brodogradnja*. 71(3), 89-118. http://dx.doi.org/10.21278/brod71306

[25] Zulqarnain, M., Fike, R., 2017. Overview of offshore drilling technologies, In book: *Encyclopedia of Maritime and Offshore Engineering*. John Wiley & Sons, Ltd., 1-12. https://doi.org/10.1002/9781118476406.emoe415

[26] ISO/TR 13624-2, 2009. Petroleum and natural gas industries—Drilling and production equipment—Part 2: Deepwater drilling riser methodologies, operations, and integrity technical report.

[27] Issa, F., Zhang, J., Sun K., Wang B., 2021. Structural analysis of jacket foundations for offshore wind turbines in transitional water. *Brodogradnja*. 72(1), 109-124. http://dx.doi.org/10.21278/brod72106

[28] DNV GL, 2014. Well System Loads - NORSOK U001.

[29] DNV GL, 2015. Wellhead Fatigue Analysis - DNVGL-RP-0142.

[30] Matlock, H., 1970. Correlation for design of laterally loaded piles in soft clay. In: Offshore Technology Conference, 1970-April. https://doi.org/10.4043/1204-MS.

Submitted: 22.02.2022.
Accepted: 29.06.2022.

Xingkun Zhou, xingkunzhou@126.com
1. Department of Marine Engineering, Dalian Maritime University, Dalian
2. National Center for International Research of Subsea Engineering Technology and Equipment, Dalian Maritime University, Dalian
Jinghao Chen, chenjinghao@bipt.edu.cn
Beijing Key Laboratory of Pipeline Critical Technology and Equipment for Deepwater Oil & Gas Development, Beijing Institute of Petrochemical Technology, Beijing
Zhengguang Ge, zxk401@gmail.com
National Center for International Research of Subsea Engineering Technology and Equipment, Dalian Maritime University, Dalian
Tong Zhao, 0520201033@bipt.edu.cn
Beijing Key Laboratory of Pipeline Critical Technology and Equipment for Deepwater Oil & Gas Development, Beijing Institute of Petrochemical Technology, Beijing
Wenhua Li, lwh992@dlmu.edu.cn
1. Department of Marine Engineering, Dalian Maritime University, Dalian
2. National Center for International Research of Subsea Engineering Technology and Equipment, Dalian Maritime University, Dalian